

A First Attempt to Calibrate the Baryonic Tully-Fisher Relation with Gas Dominated Galaxies

David V. Stark

Department of Physics and Astronomy, University of North Carolina, Chapel Hill, NC 27514

Stacy S. McGaugh, Robert A. Swaters

Department of Astronomy, University of Maryland, College Park, MD 20742

ABSTRACT

We calibrate the Baryonic Tully-Fisher (BTF) Relation using a sample of gas dominated galaxies. These determine the absolute scale of the baryonic mass–rotation speed relation independent of the choice of stellar mass estimator. We find a BTF slope of 3.94 ± 0.07 (random) ± 0.08 (systematic) and a zero point of 1.79 ± 0.26 (random) ± 0.25 (systematic). We apply this relation to estimate the stellar masses of star dominated galaxies. This procedure reproduces the trend of mass-to-light ratio with color predicted by population synthesis models. The normalization is also correct, consistent with empirical estimates of the IMF used in such models.

Subject headings: Galaxies: Kinematics and dynamics — Galaxies: Dwarf

1. Introduction

The Tully-Fisher Relation (Tully & Fisher 1977) between a galaxy’s luminosity and rotation velocity has been an important tool in establishing the extragalactic distance scale. It can also be used to set an absolute scale on mass. However, the relation between *stellar mass* and rotation velocity does not hold for all galaxies (Matthews et al. 1998; Stil & Israel 2002). Less massive, gas rich galaxies fall below the extrapolation of the relation fit to more massive, star dominated galaxies (Milgrom & Braun 1988). Continuity is restored if the correlation is made between *baryonic mass* and rotation velocity (Freeman 1999; McGaugh et al. 2000; Verheijen 2001; Bell & de Jong 2001; Gurovich et al. 2004; Pfenniger & Revaz 2005; McGaugh 2005a; Geha et al. 2006; Noordermeer & Verheijen 2007; De Rijcke et al. 2007; Begum et al. 2008). This is the Baryonic Tully-Fisher (BTF) relation.

The baryonic mass of a galaxy consists of many components, including stars, dust, and various forms of gas. The baryonic mass budget in spi-

ral galaxies is dominated by stars and cold gas: $M_b = M_s + M_g$. By comparison, other known baryonic reservoirs in these systems, such as dust and ionized gas, contain negligible amounts of mass (Bregman 2007).

By far the greatest uncertainty is presented by the stellar mass. While measuring a galaxy’s luminosity is straightforward, mapping $L \rightarrow M_s$ can be fraught (Bell & de Jong 2001; Pizagno et al. 2007; Avila-Reese et al. 2008). There are many stellar population models that provide a ratio between stellar mass and luminosity. Unfortunately, these models can yield rather different results depending on the adopted Initial Mass Function (IMF). The baryonic mass of a typical galaxy, with more mass in stars than in gas, is therefore uncertain. However, the uncertainty in the baryonic mass is substantially diminished in galaxies where more of the mass is in gas than in stars.

In this paper, we make a first attempt to use gas rich galaxies to determine the BTF relationship. We have assembled a sample with many low surface brightness and dwarf galaxies that have a higher percentage of gas than brighter high

surface brightness galaxies, whose size is comparable to those originally used to calibrate the Tully-Fisher relation (McGaugh & de Blok 1997; Schombert et al. 2001). The stellar mass is not zero, so we consider a wide range of stellar population models. The total baryonic masses of these galaxies are determined for each model. For each baryonic mass estimate, a BTF relation is derived. Since these galaxies are gas dominated, the difference in the stellar mass-to-light ratio from the different population models does not have much impact, and a consistent BTF relation emerges.

Once the BTF relation is specified by gas dominated galaxies, it can be applied to estimate the baryonic mass of star dominated galaxies. This provides a novel estimate of their stellar masses and mass-to-light ratios. These in turn provide an independent check on the predictions of population synthesis models.

In §2, we describe the galaxy sample. Its general properties are given along with a discussion of the key properties that galaxies must have to ensure a high quality sample. In §3, the methods of finding the stellar mass are discussed. In §4, the process of finding the BTF relation is presented and the best-fit relation is established. In §5, the stellar mass-to-light ratios of star dominated galaxies are determined from the BTF relation. The results are checked against population synthesis models, and limits on the IMF are discussed. Conclusions are given in §6.

2. The Sample

Our goal is to obtain a sample of gas dominated galaxies (with $M_g > M_s$) so that an absolute calibration of the BTF relation can be made independent of stellar mass estimators. It tends to be difficult to obtain high quality data for such objects, typically being both dwarf and low surface brightness. Nevertheless, thanks to the efforts of many independent workers, it is now possible to assemble a sample of such galaxies that is comparable to or larger than those originally used to calibrate the Tully-Fisher relation for distance scale work.

We have scoured the literature for galaxies that meet our criteria of gas domination and well measured rotation speed. Our galaxy sample is primarily composed from those of McGaugh (2005a — itself a compilation of many

sources) and Swaters et al. (2009), with further galaxies from other sources (de Blok et al. 2001; Matthews & Uson 2008; Uson & Matthews 2003; Begum et al. 2008; Kassin et al. 2006). Such a sample can never be complete in any rigorous sense (see §2.4). However, it is the saving grace of the Baryonic Tully-Fisher relation that all rotating galaxies seem to obey it.

2.1. Data Quality

To be included in the sample, each galaxy must satisfy certain quality criteria. The first criterion for a galaxy to be included in the sample was that it had to have rotation curve data (line-widths are not accurate enough) and its rotation curve had to reach a constant velocity. This flat velocity (v_f) is the velocity¹ used in the BTF relation. Many apparently gas rich galaxies fail to meet this criterion. It is common for the observed region of the rotation curve to rise continuously with no discernable flatness to be found. This may simply be because the measurements do not extend far enough in radius to see v_f . This is a common issue with dim dwarf galaxies, for which obtaining reliable data is challenging.

A rotation curve is considered to meet the flatness criterion if the measured velocity changes by a small amount over a defined range in radius. Quantitatively, the difference in velocity between that at three disk scale lengths and the last measured point had to be less than 15%. If measurements extended past four disk scale lengths, then the difference between the velocity at four disk scale lengths and the last measured point had to be less than 10%. Figure 1 provides examples of usable versus unusable rotation curves.

2.2. Inclination

We adopt the inclination given with the source data where possible. This is usually from a tilted ring fit, but is sometimes based on observed axis ratios. In eight cases, the inclination was not

¹Some workers use the maximum rather than flat velocity. For dwarfs, these are usually identical. For giants the difference is perceptible, but modest (McGaugh 2005b; Noordermeer & Verheijen 2007; Yegorova & Salucci 2007).

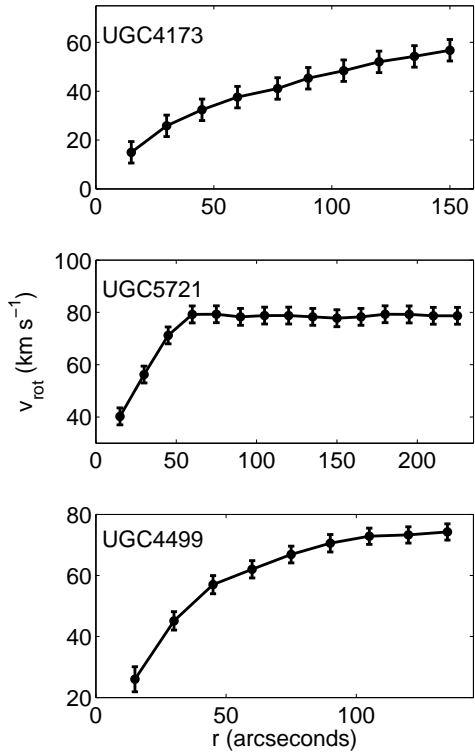


Fig. 1.— Examples of rotation curves (Swaters et al. 2009) that do and do not satisfy the flatness criterion. The rotation curve of UGC 4173 (top) rises continuously and does not meet the flatness criterion. UGC 5721 (center) is an ideal case with clear flattening of the rotational velocity. UGC 4499 marginally satisfies the flatness criterion.

given, so we estimated it with

$$\sin i = \sqrt{\frac{1 - (b/a)^2}{1 - 0.15^2}}. \quad (1)$$

The values a and b are the semi-major and semi-minor axes of the galaxy. We adopt 0.15 as the intrinsic thickness of a disk galaxy seen edge on (Kregel et al. 2004).

We select galaxies with inclinations $i > 45^\circ$. Since $v_f = v_{obs}/\sin i$, the uncertainty becomes large for smaller inclinations. As is often the case in the literature, inclination uncertainties were not reported. Given the adopted lower limit on the in-

clination, a reasonable and conservative estimate of the uncertainty on the inclination is 5° . Choosing the minimum inclination of 45° ensures the relative error in v_f from the inclination stays below 10%. This way, the uncertainty in the inclination contributes to the error budget no more than most other sources of uncertainty. Another option would have been to limit the inclination to $> 60^\circ$, reducing the relative error to less than 5%. However, this reduced the size of the galaxy sample significantly, and the number of available galaxies is already constrained heavily by the $M_g > M_s$ requirement. Limiting the inclination to this degree would have made the results excessively vulnerable to the inadequacies of small number statistics (see §4.3). As a third option, we could have allowed all galaxies with inclinations $> 30^\circ$, but this allowed the relative uncertainty to be as large as 30%, making it a major contributor to the uncertainty in v_f .

No upper limit on inclination was adopted. For galaxies with very high inclinations, the shape of the rotation curve can be affected by internal extinction. However, the outer, flat portion, which is the key quantity used in the BTF relation, is usually unaffected (Spekkens & Giovanelli 2006). Removing galaxies with $i > 80^\circ$ from our sample has a negligible effect on the results ($< 1\%$). We discuss the implications of this inclination requirement in §4.3.

2.3. Data

The primary criterion for inclusion in our fit to the BTF relation is gas dominance: $M_g > M_s$. Some galaxies always satisfy this criterion while many never do. A few skirt the boundary, depending on the stellar mass estimator employed (§3).

Table 1 provides basic information about the galaxies used in this study. Both star- and gas-dominated galaxies are tabulated in order of increasing gas mass. Though the former are not used in determining the BTF relation, we do use them to test the derived relation and stellar population models, so they are included here. We also include several low inclination galaxies. Again, these are not used in the determination of the BTF relation, but are used to test the implications of the $i > 45^\circ$ limit (see §4.3).

Many distances to galaxies were already provided in the papers in which these galaxies were found, but a search was always made for more modern or reliable distance measurements. The most common ways the distances were determined were with a Hubble flow model (H_0), the red giant branch method (TRGB), the cepheid method (CEPH), and the brightest star method (BS). Distances found with Cepheids or the red giant branch were always used if they were available, since they have been found to be more reliable indicators of a galaxy's distance (Karachentsev et al. 2004). Unless otherwise noted, the uncertainties for the red giant and Cepheid distance measurements were taken to be 10%. Likewise, the uncertainty for the brightest star method was taken as 25%. When redshifts are used as the distance indicator, we assume $H_0 = 75 \text{ km}^{-1} \text{ s}^{-1} \text{ Mpc}^{-1}$. The uncertainty in this case is taken from the spread in various flow models:

$$\sigma_D = \frac{D_{max} - D_{min}}{2}. \quad (2)$$

Here, D_{max} and D_{min} are the maximum and minimum estimates of the distance from the Hubble flow models provided by NED². It should also be noted that a number of galaxies are part of the Ursa Major cluster (Verheijen 2001). In this case, the uncertainty is that in the cluster distance (Tully & Pierce 2000). Only a few of these galaxies are gas rich, so most do not contribute to the derivation of the BTF relation.

The uncertainty in v_f varies from case to case. It depends on how well the flat velocity could be distinguished from the rest of the rotation curve, along with the uncertainty in the velocity measurements themselves. The errors predominantly fell from 1-8%, but got as high as 25% for some cases, and 60% for the most extreme (CamB).

The gas mass estimates were derived from the mass of neutral hydrogen (HI), which follows the flux from the 21 cm hydrogen emission line. We estimate the gas mass as $M_g = \frac{4}{3} M_{HI}$. The factor of 4/3 comes from the fact that hydrogen gas makes up roughly 75% of the universe. We ignore molec-

ular gas, which is not measured in most of the galaxies of concern here. In the cases where it is known (Helfer et al. 2003), it is always outweighed by either the stars or the atomic gas, and almost always by both. The work of Young & Knezek (1989) suggests that this should be generally true for galaxies in our sample. The uncertainty in the value of M_g is dominated by the distance uncertainty, but there is also some error from source noise in the measurement.

We adopt the HI masses reported by the original observers. In most cases these are synthesis observations (VLA or WSRT) or single dish maps (e.g., with the GMRT). It is common for HI fluxes to be reported without uncertainties. We adopt a typical error of 30% based on the variance between the synthesis observations and single dish estimates. This value, coupled with the uncertainty due to distance, yields the total uncertainty in M_g

$$\sigma_{M_g} = \sqrt{\left(\frac{2\sigma_D}{D} M_g\right)^2 + (0.3M_g)^2} \quad (3)$$

There is no clear indication in the data we have collected that the synthesis observations detect systematically less flux than single dish observations.

As with the gas mass, the uncertainty in luminosity is dominated by that in the distance, and again the uncertainties are seldom reported. We adopt a 10% uncertainty in the luminosity to reflect the likely disparity arising from many different measurements, instruments, and filters used in data collected from diverse sources in the literature. Therefore, the total uncertainty including the affect of distance is given by

$$\sigma_L = \sqrt{\left(\frac{2\sigma_D}{D} L\right)^2 + (0.1L)^2} \quad (4)$$

For the color, the $B-V$ band was used if available. Otherwise, $B-R$ was used. In a vast number of cases, color uncertainties are not reported. We assume them to be negligible. The consequences of this assumption are discussed in §5.2. All sources of uncertainty are added in quadrature in the analysis.

²This research has made use of the NASA/IPAC Extragalactic Database (NED) which is operated by the Jet Propulsion Laboratory, California Institute of Technology, under contract with the National Aeronautics and Space Administration.

2.4. Selection Effects

We have intentionally limited our sample to gas dominated galaxies with reasonably high quality data. These are predominantly, though not exclusively, dwarfs. Ideally, one would like a sample that is not biased towards or against any particular type of galaxy. This is an impossible ideal already broken by the distinct Tully-Fisher and Fundamental Plane relations for disk and elliptical galaxies. Among rotating disk galaxies, typical Tully-Fisher samples are numerically dominated by bright galaxies with $v_f > 100 \text{ km s}^{-1}$ simply because they are easier to see. This type of bias is unavoidable.

Perhaps the most remarkable aspect of the BTF relation is to the extent to which galaxies of very different types appear to obey it. The relation is continuous over five decades in stellar mass (McGaugh 2005a), from the fastest rotators ($\sim 300 \text{ km s}^{-1}$) to the slowest ($\sim 20 \text{ km s}^{-1}$). There is no persuasive evidence for a second parameter in the relation, as might be expected for surface brightness (Aaronson et al. 1979; Zwaan et al. 1995; McGaugh & de Blok 1998) or scale length (Courteau & Rix 1999; McGaugh 2005b). If disk galaxies do indeed all fall on a single BTF relation, as appears to be the case, then it hardly matters what portion of the relation we sample in order to calibrate it. We do of course wish to sample as broadly in velocity as possible in order to constrain the slope. Nonetheless, if the relation is both valid and universal, calibrating it with lower velocity gas rich dwarfs is no worse than calibrating it with high velocity star dominated giants as is usually done. Indeed, it has the advantage of providing an absolute normalization to the mass scale.

3. Finding the Stellar and Baryonic Mass

The true stellar mass of galaxies is unknown. We estimate M_s with a variety of stellar population models. These models take the general form

$$\log \frac{M_s}{L} = \log \Upsilon = q_B + (s_B \times color). \quad (5)$$

The constants q_B and s_B depend on the IMF and the luminosity band. We use B -band luminosities throughout here, as this is what is most commonly available. Though not as desirable as the

K -band for purposes of stellar mass estimates, this is not a substantial issue here given the selection for gas dominated galaxies. Which galaxies are determined to be gas dominated does depend on the IMF.

We utilize the stellar population synthesis models of Bell et al. (2003) and Portinari et al. (2004). These workers find that the slope s_B is fairly insensitive to the choice of IMF, the chief effect being on the normalization q_B . We used the Kroupa, Salpeter, and Kennicutt IMF models from Portinari et al. (2004), and the Scaled Salpeter, Kroupa, and Bottema IMF models from Bell et al. (2003). It should be noted that the two models give different mass-to-light ratios for what is nominally the same IMF. This appears to stem from differing treatments of brown dwarfs as well as other differences in the modeling. Nevertheless, the models are in fairly good agreement.

The population models are only expected to be valid over a finite range of color (Portinari et al. 2004). Some galaxies have such blue colors that they fall outside of this range. For lack of a better approach, we assume equation (5) holds for all colors. This does not impact the baryonic mass of gas dominated galaxies since blue colors imply low mass-to-light ratios regardless of the accuracy of equation (5). It hardly matters if Υ is tiny or merely small.

The stellar mass is calculated with

$$M_s = \Upsilon L. \quad (6)$$

The uncertainty in the mass-to-light ratio for Portinari's and Bell's population models is based on their estimates of the inherent scatter in their relations. These are 0.1 and 0.15 dex for Bell's and Portinari's models, respectively.

The total baryonic mass is simply the sum of the galaxy's gaseous and stellar components

$$M_b = M_g + M_s. \quad (7)$$

For all of these calculations, the uncertainties are added in quadrature. Tables 2 and 3 show the results from Portinari's and Bell's models. For each galaxy in the sample, the mass-to-light ratio (Υ), stellar mass (M_s), and total baryonic mass (M_b) are provided, as given by each stellar population model. We also note which galaxies qualify as gas dominated, with $M_g > M_s$. These are the galaxies we use to calibrate the BTF relation. Galaxies

that are star dominated under all population models are not included.

4. Determining the BTF Relation

4.1. Gas Dominated Subsamples

We have made six separate stellar mass estimates per galaxy. These are hereafter named for the population model-IMF combination utilized (Table 4). The idea is to only use the gas dominated galaxies to determine the BTF relation. For each sub-sample, only galaxies with gas mass greater than stellar mass ($M_g > M_s$: Tables 2 and 3) are used to make fits.

The number of galaxies in each sub-sample differs because of the different stellar mass estimators. Under one population model, a galaxy might have more gas mass than stellar mass, while under another model, the opposite could be the case. The final number of galaxies in each sub-sample is given in Table 4.

For comparison, the median mass-to-light ratios (in M_\odot/L_\odot) of the sub-samples are 0.61 for Portinari-Kroupa, 0.87 for Portinari-Salpeter, 0.51 for Portinari-Kennicutt, 0.67 for Bell-Scaled Salpeter, 0.47 for Bell-Kroupa, and 0.28 for Bell-Botttema. Note that in all cases, the typical mass-to-light ratio is less than unity. This is perhaps not surprising in that galaxies are more likely to be found to be gas dominated if they have low Υ . However, we also note that some prescriptions seem to give implausibly low mass-to-light ratios. This is particularly true of the Bell-Botttema case, which leads to the inclusion of many galaxies that would not otherwise be considered gas dominated (e.g., NGC 2998).

4.2. Linear Fits to the Subsamples

We assume the BTF relation is linear in the logarithm. If there is any curvature in the intrinsic relation, it is not apparent in our data. Therefore, fits of the form

$$\log M_b = x \log v_f + A \quad (8)$$

were made to each of the six gas-dominated subsamples. We used the OLS bisector linear fit method to determine the BTF relation coefficients. Forward and reverse fits were first conducted following the standard χ^2 minimization routine outlined in Press et al (1992, chap. 15.3), taking into

account uncertainties in both M_b and v_f . Using the coefficients from these fits and their respective uncertainties, the final OLS bisector slope and intercept were determined following the technique in Isobe et al. (1990).

The hope and intent was that the choice of stellar population model would have a little effect on the total baryonic mass, and in turn, on the derived BTF relation. Table 4 shows the results of the fit for each gas rich sub-sample. One can immediately see that indeed the population model does not have a drastic effect on the BTF relation.

As a further test, we considered the selection criterion $M_g > 2M_s$ to further suppress any dependence on the choice of population model. The results are indistinguishable. Rather few galaxies survive this very restrictive selection criterion, so we do not consider this case further.

The choice of stellar mass estimator has an impact on the quality of the fits. Three cases (the Portinari-Kroupa, Portinari-Salpeter, and Bell-Scaled Salpeter sub-samples) have reasonable reduced χ^2 values (Table 4). These are shown in Figure 2. The other cases look similar, albeit with worse formal χ^2 . In order to determine a single calibration for the BTF relation, a weighted average is made of the coefficients from the three illustrated sub-samples, with weights given by

$$w = \frac{1}{|\chi^2 - 1|}. \quad (9)$$

The resulting BTF relation is

$$\log M_b = 3.94 \log v_f + 1.79. \quad (10)$$

The formal random uncertainty in this OLS bisector fit is ± 0.07 in the slope and ± 0.26 in the intercept. In addition to the random errors, we attempt to estimate the systematic uncertainties. The choice of population model still plays a some role in constraining the intercept of the BTF relation, as the stellar mass is minimized but not zero. Likewise, there is some systematic uncertainty in the slope that seems to depend on the inclination cut off. This will be discussed in further detail in §4.3. For now, the estimated magnitude of the systematic uncertainties are ± 0.08 in the slope and ± 0.25 in the intercept.

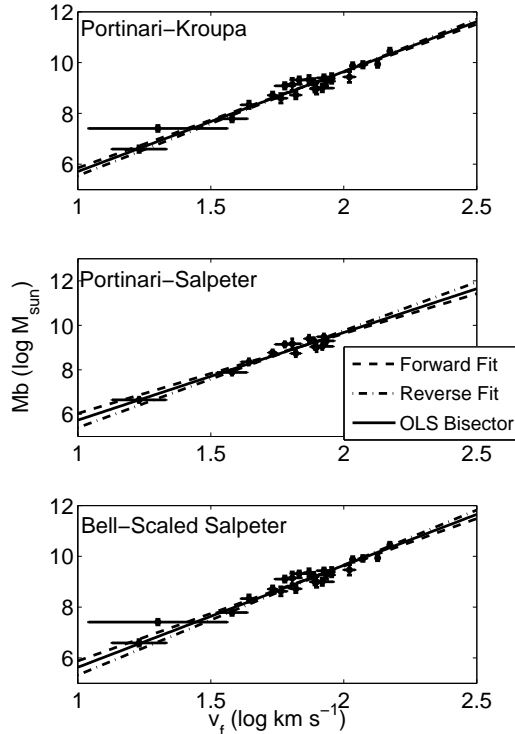


Fig. 2.— Fits of the BTFR relation to the three gas dominated sub-samples with good χ^2_ν .

4.3. Systematic Effects and the Inclination Limit

We have investigated how our sample selection criteria affect the result. The choice of the stellar mass estimator, the line between star and gas domination, and the velocity measure employed (v_f vs. v_{max}) all make little difference. The limit on inclination, $i > 45^\circ$, has a mild effect on the slope, discussed further below. While variations in the sample selection makes no net systematic difference to the intercept, the range of variation does give some handle on the possible amplitude of the systematic error.

The formal error in the intercept has been determined by bootstrap resampling of the data. Approximately 95% of the data fall within 2σ of the best fit value. As is usually the case for astronomical data, it is rather harder to estimate the systematic uncertainty. By examining the varia-

tion in the zero points from the fits to the various subsamples, forward and reverse OLS as well as the bisector method, we estimate a systematic uncertainty in the intercept of ± 0.25 . This covers the full range of variation, so is rather conservative.

For the uncertainty in slope, there does seem to be a mild but systematic dependence on the imposed inclination limit. Some cut off on the inclination of galaxies included in the sample is necessary, as the velocity depends on $1/\sin(i)$. Face on galaxies have very large uncertainties due to inclination. Inclusion of such data will bias the determination of the slope Jefferys (1980), so we impose a limit to combat this effect. This inclination limit is chosen to provide a middle ground between data quality and sample size (see §2.2). As a check, we vary the inclination limit imposed on the gas dominated sub-samples, letting the minimum range from 0 to 70° . The BTFR relation is derived for each inclination cut. The bisector slope and sample size of each fit is shown in Figure 3.

The slope is relatively stable from no cut to an inclination limit of $i > 55^\circ$, varying between 3.76 and 3.95. For the most part, the magnitude of these variations are comparable to the uncertainty in the fits. For higher inclination cuts, the slope becomes much larger. The cause of this is the drastic reduction in sample size, as seen in figure 4. For the last inclination cut, only 15% of the sample remains, leaving only 3 to 6 galaxies depending on the population model used. Therefore, we reach a point where restricting the inclination too much simply leads to small number statistics. This effect sets in around $i_{min} \approx 60^\circ$, where the slope strongly deviates from the mean, and the uncertainty drastically increases. This is most clearly seen in the transition from $i_{min} = 60^\circ$ to $i_{min} = 65^\circ$. Over this range, the sample size is effectively cut in half. This leaves one galaxy with a low relative velocity, but it has a very large uncertainty, effectively leaving nothing to constrain the low end of the fit. Choosing $i > 45^\circ$ keeps us well away from this region where small number statistics issues like this one take over. Accounting for the variation in best fit slope with the choice of inclination limit gives a systematic uncertainty of 0.08, discounting the sharp change due to small numbers at very large inclination limits.

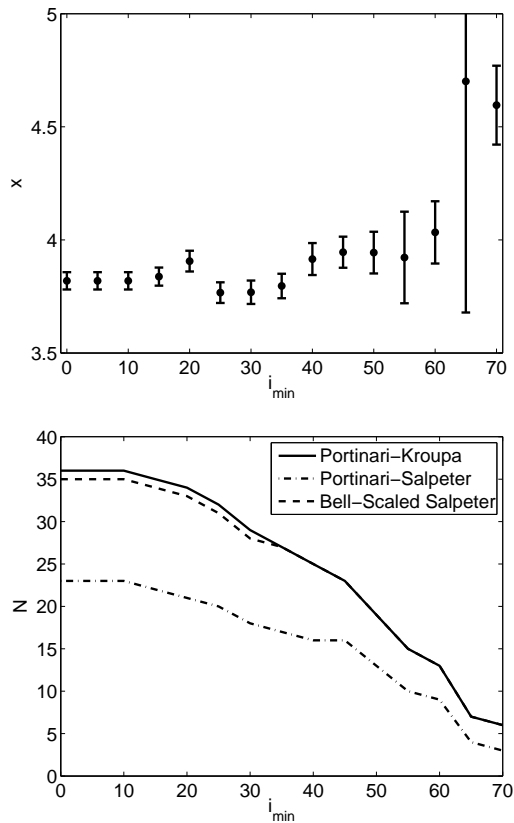


Fig. 3.— Derived slope (x) of the BTF fit (left) and number of galaxies (right) versus the minimum inclination limit imposed upon the sample.

5. Stellar Masses from the BTF Relation

The Baryonic Tully-Fisher Relation derived from gas dominated galaxies provides a novel estimator of a galaxy’s total baryonic mass. The observed rotation speed v_f is in effect a measure of baryonic mass. For a galaxy of known distance, the stellar mass can be found by subtracting off the observed gas mass:

$$M_s = M_b - M_g. \quad (11)$$

Dividing this by the luminosity gives the mass-to-light ratio, Υ .

Table 5 shows the baryonic mass, stellar mass, and mass-to-light ratio indicated by the BTF relation. Note that this relation, once derived, can be applied to any rotating galaxy. This provides an estimate of the stellar mass for the star dom-

inated galaxies in Table 1 that is independent of population synthesis models.

5.1. Testing Population Synthesis Models

The stellar mass-to-light ratios determined from the BTF relation provide a means of testing the population synthesis models. These models utilize our knowledge of stellar evolution and prescriptions for galactic star formation histories to predict the color- Υ relation. We utilize dynamical information in the form of the BTF relation to estimate the mass-to-light ratios of star dominated galaxies.

The methods and data involved in this process are distinct and very nearly independent. They are not completely independent as population synthesis models have been used in the BTF calibration. However, as revealed by Table 4, the differences in stellar mass given by the different population models have only a negligible impact on the BTF. By construction, the gas mass dominates the calibration. Consequently, this may be as close as it is possible to get to an independent test of the predictions of population synthesis models.

We detect a clear correlation between mass-to-light ratio and color. This is expected in the models of Portinari et al. (2004) and Bell et al. (2003), which are consistent in predicting a slope of $s_B = 1.7$ for the color- Υ relation. Our data are consistent with this slope (Figure 4). This appears to be a remarkable confirmation of a basic prediction of population synthesis models.

5.2. Constraining the IMF

The main uncertainty in population models is from the IMF. Here we apply our calibration of the BTF relation to derive our own color- Υ relation. This provides an independent constraint on the IMF.

We fit the IMF normalization q_B of equation (5) to the data in Figure 4. The slope of the data is consistent with the expectation of the models, within the uncertainties. To provide a direct comparison to the IMF of the models, we fix the slope and fit only for the normalization q_B . In this process, we utilize only those star dominated galaxies with $B - V$ colors that were not part of the three sub-samples used to calibrate the BTF relation (§2.4).

The BTF-derived IMF coefficient provides a constraint on the IMF. We find $q_B = -0.94 \pm 0.20$ such that, in the mean,

$$\log \Upsilon = 1.7(B - V) - 0.94. \quad (12)$$

The BTF-derived values of Υ and the fit (equation 12) are shown in Figure 4.

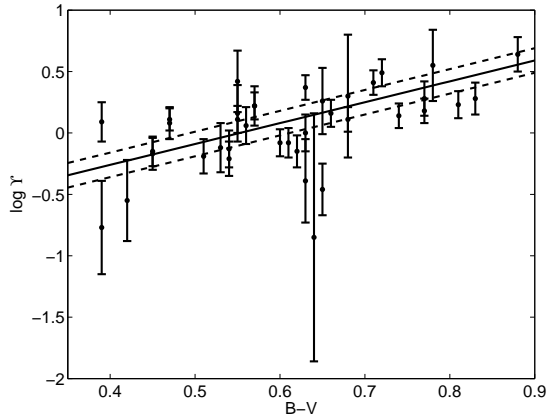


Fig. 4.— The mass-to-light ratios Υ derived from the BTF relation as a function of $B - V$ color. The line represents a fit to these data. Only star dominated galaxies are used, not the gas dominated galaxies used to determine the BTF. The normalization is the only fitting parameter; the slope is fixed to the value predicted by stellar population models (Bell et al. 2003; Portinari et al. 2004). The dotted lines show the uncertainty in the fit.

The constraint derived here on the IMF agrees most closely with the Bell-Scaled Salpeter or Portinari-Kroupa models. This is not a strong statement, as the uncertainties allow many of the IMFs considered by both Bell et al. (2003) and Portinari et al. (2004). However, it does suggest that the IMF is normal, and not outrageously different than assumed in population synthesis models. Indeed, the more extreme IMFs, both heavy (Portinari-Salpeter) and light (Bell-Botttema), are disfavored.

The scatter in Υ is 0.20 dex. Roughly half of this can be attributed to observational uncertainties, leaving an intrinsic scatter of ~ 0.14 in the mass-to-light ratio. This is consistent with the intrinsic scatter expected by Bell et al. (2003) and Portinari et al. (2004).

As mentioned in §2.3, we take the color uncertainties to be negligible as they are widely unreported. We test the implication of this assumption by repeating the linear fits to find q_B but giving the $B - V$ values uniform uncertainties. The IMF normalization q_B goes down by 0.02 for $\sigma_{B-V} = 0.05$, then drops by 0.04 for every addition of 0.05 to the color uncertainty up to $\sigma_{B-V} = 0.2$, the largest value considered. It seems unlikely that the average uncertainty in the colors would be larger than this, so the effect is likely to be modest. However, we can not exclude the possibility of a larger effect if the galaxies with extremal colors also have large uncertainties.

6. Conclusions

We have fit the Baryonic Tully-Fisher relation for a sample of gas dominated galaxies. We obtain an absolute calibration of the baryonic mass-rotation speed relation that is effectively independent of the choice of stellar mass estimator. For the data assembled here, we find a BTF relation with a slope $x = 3.94 \pm 0.07$ (random) ± 0.08 (systematic) and an intercept $A = 1.79 \pm 0.26$ (random) ± 0.25 (systematic).

We use our derived BTF relation to estimate the baryonic and stellar masses of a sample of star dominated galaxies independent of the calibration sample. The stellar mass-to-light ratios found in this way are in remarkably good agreement with the predictions of population synthesis models (Bell et al. 2003; Portinari et al. 2004). The expected trend of mass-to-light ratio with color is reproduced, and the absolute scale is consistent with the best estimates of the IMF.

To place a constraint on the IMF, we have treated the coefficient q_B of the color-mass-to-light ratio relation (equation 5) as a fit parameter. We obtain $q_B = -0.94 \pm 0.20$. This is consistent with a Kroupa, Kennicutt, or Scaled Salpeter IMF. When observational uncertainty is subtracted, the amount of scatter in the color-mass-to-light ratio relation is consistent with that of past models, and does not exceed that expected from variation in the star formation histories of different galaxies. This suggests that variation in the IMF does not contribute significantly to the scatter. Perhaps the IMF tends to some universal value when averaged over the many individual star

formation events necessary to build up the stellar mass of bright galaxies.

A common interpretation of the Tully-Fisher relation is that baryonic mass scales with dark mass, and the observed velocity is proportional to the characteristic halo velocity. These assumptions can not strictly hold, as the observed slope deviates significantly from that ($x = 3$) of the theoretical halo mass-velocity relation for CDM halos (Steinmetz & Navarro 1999). Perhaps the effective baryon fraction varies systematically with circular velocity, or some other physics underlies the relation.

This study was a first attempt to calibrate the BTF relation using gas dominated galaxies. However, in its current state, it is not free from potential statistical uncertainties (§4.3). This is quite evident by our measure of χ^2_ν as a function of inclination limit. Even a small adjustment to the sample can change the fit, though for the most part we consider this to be within tolerable limits. Future attempts to calibrate the BTF relation would benefit from a larger sample of gas rich galaxies.

The work of SSM is supported in part by NSF grant AST 0505956.

REFERENCES

- Aaronson, M., Huchra, J., & Mould, J. 1979, *ApJ*, 229, 1
- Avila-Reese, V., Zavala, J., Firmani, C., & Hernández-Toledo, H. M. 2008, *AJ*, 136, 1340
- Begeman, K. G., Broeils, A. H., & Sanders, R. H. 1991, *MNRAS*, 249, 523
- Begum, A., & Chengalur, J. N. 2003, *A&A*, 409, 879
- Begum, A., Chengalur, J. N., & Karachentsev, I. D. 2005, *A&A*, 433, L1
- Begum, A., Chengalur, J. N., Karachentsev, I. D., & Sharina, M. E. 2008, *MNRAS*, 386, 138
- Begum, A., Chengalur, J. N., Kennicutt, R. C., Karachentsev, I. D., & Lee, J. C. 2008, *MNRAS*, 383, 809
- Bell, E. F., & de Jong, R. S. 2001, *ApJ*, 550, 212
- Bell, E. F., McIntosh, D. H., Katz, N., & Weinberg, M. D. 2003, *ApJS*, 149, 289
- Bregman, J. N. 2007, *ARA&A*, 45, 221
- Courteau, S., & Rix, H.-W. 1999, *ApJ*, 513, 561
- de Blok, W. J. G., & McGaugh, S. S. 1998, *ApJ*, 508, 132
- de Blok, W. J. G., McGaugh, S. S., & Rubin, V. C. 2001, *AJ*, 122, 2396
- De Rijcke, S., Zeilinger, W. W., Hau, G. K. T., Prugniel, P., & Dejonghe, H. 2007, *ApJ*, 659, 1172
- Freeman, K. C. 1999, *The Low Surface Brightness Universe*, 170, 3
- Geha, M., Blanton, M. R., Masjedi, M., & West, A. A. 2006, *ApJ*, 653, 240
- Gurovich, S., McGaugh, S. S., Freeman, K. C., Jerjen, H., Staveley-Smith, L., & De Blok, W. J. G. 2004, *Publications of the Astronomical Society of Australia*, 21, 412
- Helfer, T. T., Thornley, M. D., Regan, M. W., Wong, T., Sheth, K., Vogel, S. N., Blitz, L., & Bock, D. C.-J. 2003, *ApJS*, 145, 259
- Isobe, T., Feigelson, E. D., Akritas, M. G., & Babu, G. J. 1990, *ApJ*, 364, 104
- Jackson, D. C., Skillman, E. D., Cannon, J. M., & Côté, S. 2004, *AJ*, 128, 1219
- Jefferys, W. H. 1980, *AJ*, 85, 177
- Karachentsev, I. D. 2005, *AJ*, 129, 178
- Karachentsev, I. D., Karachentseva, V. E., Huchtmeier, W. K., & Makarov, D. I. 2004, *AJ*, 127, 2031
- Kassin, S. A., de Jong, R. S., & Pogge, R. W. 2006, *ApJS*, 162, 80
- Kregel, M., van der Kruit, P. C., & Freeman, K. C. 2004, *MNRAS*, 351, 1247
- Matthews, L. D., van Driel, W., & Gallagher, J. S., III 1998, *AJ*, 116, 2196
- Matthews, L. D., & Uson, J. M. 2008, *AJ*, 135, 291

- McGaugh, S. S. 2005, *ApJ*, 632, 859
- McGaugh, S. S. 2005, *Physical Review Letters*, 95, 171302
- McGaugh, S. S., & de Blok, W. J. G. 1997, *ApJ*, 481, 689
- McGaugh, S. S., & de Blok, W. J. G. 1998, *ApJ*, 499, 41
- McGaugh, S. S., Schombert, J. M., Bothun, G. D., & de Blok, W. J. G. 2000, *ApJ*, 533, L99
- Milgrom, M., & Braun, E. 1988, *ApJ*, 334, 130
- Noordermeer, E., & Verheijen, M. A. W. 2007, *MNRAS*, 381, 1463
- Pfenniger, D., & Revaz, Y. 2005, *A&A*, 431, 511
- Pizagno, J., et al. 2007, *AJ*, 134, 945
- Portinari, L., Sommer-Larsen, J., & Tantalo, R. 2004, *MNRAS*, 347, 691
- Press, W. H., Teukolsky, S. A., Vetterling, W. T., & Flannery, B. P., *Numerical Recipes in C*, 2nd Ed, Cambridge University Press, New York, 1992
- Sanders, R. H. 1996, *ApJ*, 473, 117
- Schombert, J. M., McGaugh, S. S., & Eder, J. A. 2001, *AJ*, 121, 2420
- Spekkens, K., & Giovanelli, R. 2006, *AJ*, 132, 1426
- Steinmetz, M., & Navarro, J. F. 1999, *ApJ*, 513, 555
- Swaters, R. A., Sancisi, R., van Albada, T. S., & van der Hulst, J. M. 2009, *A&A*, 493, 871
- Stil, J. M., & Israel, F. P. 2002, *A&A*, 389, 42
- Tully, R. B., & Fisher, J. R. 1977, *A&A*, 54, 661
- Tully, R. B., & Pierce, M. J. 2000, *ApJ*, 533, 744
- Uson, J. M., & Matthews, L. D. 2003, *AJ*, 125, 2455
- Verheijen, M. A. W. 2001, *ApJ*, 563, 694
- Warren, B. E., Jerjen, H., & Koribalski, B. S. 2004, *AJ*, 128, 1152
- Yegorova, I. A., & Salucci, P. 2007, *MNRAS*, 377, 507
- Young, J. S., & Knezek, P. M. 1989, *ApJ*, 347, L55
- Zwaan, M. A., van der Hulst, J. M., de Blok, W. J. G., & McGaugh, S. S. 1995, *MNRAS*, 273, L35

TABLE 1
GALAXY SAMPLE

Galaxy	D^a (Mpc)	σ_D	Method	Ref.	i (degrees)	v_f (km s ⁻¹)	σ_{v_f}	M_g (log M_\odot)	L_B (log L_\odot)	Color	Band
(1)	(2)	(3)	(4)	(5)	(6)	(7)	(8)	(9)	(10)	(11)	(12)
DDO210	0.94	0.09	TRGB	9	50 ^b	17	4	6.51	6.38	0.25	<i>B - V</i>
CamB	3.34	0.33	TRGB	4	65	20	12	7.22	6.93	0.58	<i>B - V</i>
WLM	0.95	0.1	TRGB	10	64	38	5	7.60	7.77	0.29	<i>B - V</i>
KK98251	5.9	1.48	BS	9	62	36	6	8.06	8.05	0.79	<i>B - V</i>
NGC3741	3.0	0.3	TRGB	8	46 ^b	44	3	8.3	7.52	0.38	<i>B - V</i>
UGC8550	5.1	1.28	BS	9	90	58	3	8.34	7.88	1.26	<i>B - R</i>
DDO168	4.33	0.43	TRGB	4	60 ^b	54	2	8.60	8.46	0.32	<i>B - V</i>
NGC3109	1.33	0.13	TRGB	2	86	66	3	8.70	7.54	0.47	<i>B - V</i>
UGC8490	4.65	0.47	TRGB	9	50	78	3	8.84	8.91	0.48	<i>B - R</i>
UGC3711	7.9	0.79	TRGB	9	60	95	3	8.89	8.80	1.05	<i>B - R</i>
F565V2	48	6.65	H0	3	60	83	8	8.91	8.36	0.51	<i>B - V</i>
UGC5721	6.5	1.63	AVG	9	61	79	3	8.93	8.55	0.63	<i>B - R</i>
UGC3851	3.19	0.32	TRGB	9	59	60	5	8.97	8.53	0.88	<i>B - R</i>
NGC2683	7.73	2.32	SBF	1	82	155	5	9.06	10.14	0.65	<i>B - V</i>
UGC6667	18.6	1.93	GROUP	5	90	85	3	9.06	9.57	0.65	<i>B - V</i>
UGC6923	18.6	1.93	GROUP	5	65	81	5	9.06	9.50	0.42	<i>B - V</i>
IC2574	4.02	0.4	TRGB	4	58 ^b	68	5	9.08	9.16	0.42	<i>B - V</i>
UGC9211	12.6	3.3	GROUP	11	48	64	5	9.12	8.39	0.72	<i>B - R</i>
NGC1560	3.45	0.35	TRGB	2	80	77	1	9.10	8.67	0.57	<i>B - V</i>
NGC5585	5.7	1.45	BS	1	51	90	2	9.15	9.13	0.46	<i>B - V</i>
UGC7321	10	3	AVG	12	90	105	5	9.20	9.03	0.97	<i>B - R</i>
UGC6818	18.6	1.93	GROUP	5	68 ^b	72	6	9.16	9.41	0.43	<i>B - V</i>
NGC7793	3.91	0.39	TRGB	1	47	95	10	9.20	9.73	0.63	<i>B - V</i>
UGC4499	13	2.35	H0	11	50	74	3	9.20	9.02	0.72	<i>B - R</i>
IC 2233	10.4	1.04	TRGB	7	89	84	5	9.20	9.29	0.67	<i>B - R</i>
NGC3972	18.6	1.93	GROUP	5	77	133	3	9.24	9.99	0.55	<i>B - V</i>
F583-1	32	5.25	H0	13	63	86	6	9.20	8.67	0.39	<i>B - V</i>
NGC4085	18.6	1.93	GROUP	5	82	136	6	9.27	10.07	0.47	<i>B - V</i>
NGC6503	5.27	0.53	TRGB	2	74	115	1	9.28	9.58	0.57	<i>B - V</i>
NGC3877	18.6	1.93	GROUP	5	76	170	1	9.30	10.45	0.68	<i>B - V</i>
NGC4138	18.6	1.93	GROUP	5	53	148	4	9.30	10.07	0.81	<i>B - V</i>
NGC247	3.65	0.37	TRGB	1	74	106	2	9.34	9.77	0.54	<i>B - V</i>
UGC6973	18.6	1.93	GROUP	5	71	174	9	9.39	9.95	0.88	<i>B - V</i>
NGC3917	18.6	1.93	GROUP	5	79	137	1	9.41	10.21	0.6	<i>B - V</i>
UGC6917	18.6	1.93	GROUP	5	57	111	5	9.46	9.74	0.53	<i>B - V</i>
NGC4217	18.6	1.93	GROUP	5	86	178	1	9.56	10.44	0.77	<i>B - V</i>
NGC4051	18.6	1.93	GROUP	5	49	160	7	9.57	10.57	0.62	<i>B - V</i>
NGC3953	18.6	1.93	GROUP	5	62	223	3	9.59	10.62	0.71	<i>B - V</i>
NGC4010	18.6	1.93	GROUP	5	76 ^b	123	3	9.59	9.96	0.54	<i>B - V</i>
NGC4013	18.6	1.93	GROUP	5	80 ^b	177	7	9.62	10.32	0.83	<i>B - V</i>
UGC6983	18.6	1.93	GROUP	5	49	108	2	9.62	9.69	0.45	<i>B - V</i>
NGC4100	18.6	1.93	GROUP	5	73	160	9	9.64	10.41	0.63	<i>B - V</i>
NGC2403	3.18	0.32	CEPH	2	60	134	1	9.65	9.88	0.39	<i>B - V</i>
NGC3949	18.6	1.93	GROUP	5	55	165	10	9.68	10.38	0.39	<i>B - V</i>
NGC4183	18.6	1.93	GROUP	5	82	111	2	9.69	10.11	0.39	<i>B - V</i>
F5741	96	6.3	H0	3	82 ^b	99	1	9.69	9.57	1.06	<i>B - R</i>
F5681	85	10.1	H0	3	46	118	4	9.70	9.45	0.58	<i>B - V</i>
NGC2903	8.9	2.23	BS	2	63	181	4	9.78	10.47	0.55	<i>B - V</i>
NGC3521	9.3	5	H0	1	61	190	15	9.84	10.42	0.68	<i>B - V</i>

TABLE 1—*Continued*

Galaxy	D^a (Mpc)	σ_D	Method	Ref.	i (degrees)	v_f (km s $^{-1}$)	σ_{v_f}	M_g (log M_\odot)	L_B (log L_\odot)	Color	Band
(1)	(2)	(3)	(4)	(5)	(6)	(7)	(8)	(9)	(10)	(11)	(12)
NGC3769	18.6	1.93	GROUP	5	70	118	5	9.88	9.99	0.64	$B - V$
NGC3893	18.6	1.93	GROUP	5	49	176	9	9.91	10.49	0.56	$B - V$
NGC1003	12.3	3.41	H0	1	67	112	3	9.95	10.21	0.55	$B - V$
NGC3726	18.6	1.93	GROUP	6	53	168	2	9.95	10.58	0.45	$B - V$
NGC 157	20.16	4.65	H0	7	45	120	17	9.99	10.34	0.62	$B - V$
NGC5033	12.4	3.35	H0	1	64	195	4	10.00	10.31	0.55	$B - V$
NGC5907	11.0	3.58	H0	1	90	215	2	10.04	10.38	0.78	$B - V$
NGC7331	15.1	1.51	CEPH	2	75	238	2	10.05	10.74	0.63	$B - V$
NGC4088	18.6	1.93	GROUP	5	69	170	5	10.06	10.61	0.51	$B - V$
NGC4157	18.6	1.93	GROUP	5	82	185	1	10.06	10.46	0.66	$B - V$
NGC3992	18.6	1.93	GROUP	5	56	241	4	10.12	10.65	0.72	$B - V$
NGC3198	14.45	1.45	CEPH	2	74	149	1	10.17	10.32	0.43	$B - V$
NGC2998	67	7	H0	1	63	212	3	10.48	10.95	0.45	$B - V$
NGC801	83	8.1	H0	1	80	216	1	10.49	10.90	0.61	$B - V$
NGC5533	56	7.05	H0	1	55	240	6	10.51	10.78	0.77	$B - V$
NGC2841	14.1	1.41	CEPH	2	70	287	4	10.58	11.28	0.74	$B - V$
NGC6674	49	7.5	H0	1	46	242	2	10.59	10.83	0.57	$B - V$
UGC2885	82	6.95	H0	1	64	298	1	10.73	11.35	0.47	$B - V$
GR8	2.1	0.21	TRGB	14	28	25	5	7.10	6.99	0.38	$B - V$
DDO154	4.3	1.08	BS	3	28	48	6	8.72	7.76	0.32	$B - V$
UGC7278	2.94	0.29	TRGB	9	30	80	2	8.88	9.05	0.8	$B - R$
UGC5846	13.2	3.55	GROUP	11	30	51	7	8.97	8.47	0.39	$B - R$
UGC4325	10.1	1.85	H0	11	41	92	2	9.00	9.16	0.68	$B - R$
E215g9	5.25	0.41	TRGB	15	36	51	5	9.03	7.56	1.02	$B - V$
F571V1	79	9.75	H0	3	35	83	5	9.21	9.00	0.55	$B - V$
F563V2	61	7.05	H0	3	29	111	5	9.51	9.48	0.51	$B - V$
F568V1	80	9.55	H0	3	40	124	5	9.53	9.34	0.57	$B - V$
F5631	45	6.2	H0	3	11	111	1	9.59	9.15	0.64	$B - V$
UGC6446	18.6	1.93	GROUP	5	24	83	3	9.64	9.56	0.39	$B - V$
UGC1230	51	7	H0	3	16	133	2	9.91	9.51	0.54	$B - V$
UGC128	60	8.4	H0	3	21	130	2	9.96	9.72	0.60	$B - V$

NOTE.—Column (1) gives the galaxy’s name; Column (2) gives the distance used for this paper; Column (3) gives the uncertainty for the distance; Column (4) gives the method used to estimate the distance; Column (5) gives the corresponding reference to the distance value; Column (6) gives the inclination of the galaxy; Column (7) gives the flat rotational velocity of the galaxy; Column (8) gives the uncertainty to the velocity measurement; Column (9) gives gas mass of the galaxy; Column (10) gives the B band luminosity of the galaxy; Column (11) gives the color measurement; Column (12) gives the band corresponding to each color measurement.

^aDistance estimation methods: H_0 : Hubble flow with Virgo Cluster effect; CEPH: cepheid; TRGB: tip of red giant branch; GROUP: average distance of galaxy’s group; BS: brightest stars; AVG: average of several measurements

^bInclination estimated with equation (1)

References. — (1) Sanders (1996); (2) Begeman et al. (1991); (3) de Blok & McGaugh (1998); (4) Karachentsev (2005); (5) Tully & Pierce (2000); (6) Kassin et al. (2006); (7) Matthews & Uson (2008); (8) Begum et al. (2005); (9) Karachentsev et al. (2004); (10) Jackson et al. (2004); (11) Swaters et al. (2009); (12) Uson & Matthews (2003); (13) de Blok et al. (2001); (14) Begum & Chengalur (2003); (15) Warren et al. (2004)

TABLE 2
 MASS RESULTS FROM PORTINARI'S POPULATION MODELS

Galaxy	Kroupa IMF				Salpeter IMF				Kennicutt IMF			
	Υ (M_{\odot}/L_{\odot})	M_b ($\log M_{\odot}$)	σ_{M_b}	$M_g > M_s?$	Υ (M_{\odot}/L_{\odot})	M_b ($\log M_{\odot}$)	σ_{M_b}	$M_g > M_s?$	Υ (M_{\odot}/L_{\odot})	M_b ($\log M_{\odot}$)	σ_{M_b}	$M_g > M_s?$
DDO210	0.31	6.61	0.13	Y	0.52	6.66	0.12	Y	0.26	6.59	0.14	Y
CamB	1.14	7.41	0.12	Y	1.89	7.51	0.12	Y	0.92	7.38	0.12	Y
WLM	0.37	7.81	0.12	Y	0.61	7.90	0.12	Y	0.30	7.78	0.12	Y
NGC3741	0.52	8.36	0.15	Y	0.87	8.38	0.14	Y	0.42	8.36	0.15	Y
UGC8550	2.32	8.60	0.19	Y	3.77	8.71	0.19	N	1.86	8.56	0.19	Y
DDO168	0.41	8.73	0.13	Y	0.69	8.79	0.12	Y	0.33	8.71	0.13	Y
NGC3109	0.74	8.70	0.15	Y	1.23	8.71	0.14	Y	0.60	8.69	0.15	Y
UGC8490	0.28	8.96	0.13	Y	0.46	9.03	0.12	Y	0.23	8.94	0.13	Y
UGC3711	1.32	9.21	0.12	N	2.14	9.33	0.13	N	1.06	9.16	0.12	Y
F565V2	0.86	9.02	0.15	Y	1.44	9.07	0.14	Y	0.70	9.00	0.15	Y
UGC5721	0.42	9.00	0.22	Y	0.69	9.04	0.21	Y	0.34	8.99	0.22	Y
UGC3851	0.83	9.08	0.13	Y	1.35	9.14	0.12	Y	0.67	9.06	0.13	Y
UGC6923	0.61	9.49	0.13	N	1.02	9.64	0.15	N	0.49	9.43	0.13	N
IC2574	0.61	9.32	0.12	Y	1.02	9.43	0.12	N	0.49	9.28	0.12	Y
UGC9211	0.54	9.13	0.24	Y	0.88	9.16	0.23	Y	0.43	9.13	0.24	Y
NGC1560	1.09	9.26	0.12	Y	1.82	9.33	0.12	Y	0.89	9.23	0.13	Y
NGC5585	0.71	9.37	0.19	Y	1.19	9.48	0.19	N	0.58	9.34	0.19	Y
UGC7321	1.06	9.41	0.21	Y	1.73	9.51	0.22	N	0.85	9.37	0.21	Y
UGC6818	0.63	9.49	0.12	N	1.06	9.62	0.14	N	0.51	9.44	0.12	Y
UGC4499	0.54	9.33	0.16	Y	0.88	9.40	0.15	Y	0.43	9.31	0.17	Y
IC 2233	0.47	9.40	0.12	Y	0.77	9.49	0.12	Y	0.38	9.37	0.12	Y
F583-1	0.54	9.30	0.17	Y	0.90	9.33	0.16	Y	0.44	9.29	0.17	Y
NGC6503	1.09	9.78	0.14	N	1.82	9.95	0.15	N	0.89	9.72	0.13	N
UGC6917	0.93	9.90	0.13	N	1.56	10.06	0.15	N	0.76	9.85	0.13	N
NGC4010	0.97	10.11	0.14	N	1.62	10.27	0.15	N	0.79	10.05	0.13	N
UGC6983	0.68	9.87	0.12	Y	1.14	9.98	0.13	N	0.56	9.83	0.12	Y
NGC2403	0.54	9.94	0.12	Y	0.90	10.06	0.13	N	0.44	9.89	0.12	Y
NGC4183	0.54	10.07	0.13	N	0.90	10.22	0.14	N	0.44	10.02	0.13	N
F5741	1.34	10.00	0.11	N	2.18	10.12	0.12	N	1.08	9.95	0.11	Y
F5681	1.14	9.94	0.13	Y	1.89	10.04	0.13	Y	0.92	9.91	0.13	Y
NGC3769	1.43	10.34	0.13	N	2.39	10.49	0.15	N	1.16	10.28	0.13	N
NGC1003	1.01	10.40	0.21	N	1.68	10.56	0.23	N	0.82	10.35	0.21	N
NGC5033	1.01	10.49	0.21	N	1.68	10.65	0.23	N	0.82	10.43	0.21	N
NGC3198	0.63	10.45	0.12	Y	1.06	10.57	0.13	N	0.51	10.41	0.12	Y
NGC2998	0.68	10.96	0.14	N	1.14	11.12	0.15	N	0.56	10.90	0.13	N
NGC6674	1.09	11.05	0.15	N	1.82	11.21	0.17	N	0.89	11.00	0.15	N

NOTE.—Not shown here are galaxies that are star dominated for all population models. They are not used to determine the BTF relation.

TABLE 3
 MASS RESULTS FROM BELL'S POPULATION MODELS

Galaxy	Scaled-Salpeter IMF				Kroupa IMF				Bottema IMF			
	Υ (M_{\odot}/L_{\odot})	M_b ($\log M_{\odot}$)	σ_{M_b}	$M_g > M_s?$	Υ (M_{\odot}/L_{\odot})	M_b ($\log M_{\odot}$)	σ_{M_b}	$M_g > M_s?$	Υ (M_{\odot}/L_{\odot})	M_b ($\log M_{\odot}$)	σ_{M_b}	$M_g > M_s?$
DDO210	0.31	6.61	0.13	Y	0.22	6.58	0.14	Y	0.12	6.56	0.14	Y
CamB	1.16	7.42	0.11	Y	0.82	7.37	0.12	Y	0.46	7.31	0.13	Y
WLM	0.36	7.81	0.11	Y	0.26	7.76	0.12	Y	0.15	7.71	0.13	Y
NGC3741	0.52	8.36	0.15	Y	0.37	8.35	0.15	Y	0.21	8.34	0.15	Y
UGC8550	2.65	8.63	0.18	Y	1.88	8.56	0.18	Y	1.06	8.48	0.20	Y
DDO168	0.41	8.73	0.13	Y	0.29	8.70	0.13	Y	0.16	8.66	0.14	Y
NGC3109	0.75	8.70	0.15	Y	0.53	8.69	0.15	Y	0.30	8.68	0.15	Y
UGC8490	0.36	8.99	0.12	Y	0.26	8.95	0.12	Y	0.14	8.91	0.14	Y
UGC3711	1.55	9.24	0.10	N	1.10	9.17	0.11	Y	0.62	9.07	0.11	Y
F565V2	0.88	9.02	0.15	Y	0.62	8.99	0.15	Y	0.35	8.96	0.16	Y
UGC5721	0.53	9.02	0.21	Y	0.37	9.00	0.22	Y	0.21	8.97	0.23	Y
UGC3851	1.00	9.10	0.12	Y	0.71	9.07	0.13	Y	0.40	9.03	0.14	Y
UGC6923	0.61	9.49	0.11	N	0.43	9.40	0.11	N	0.24	9.28	0.11	Y
IC2574	0.61	9.32	0.11	Y	0.43	9.26	0.11	Y	0.24	9.19	0.13	Y
UGC9211	0.67	9.14	0.23	Y	0.47	9.13	0.24	Y	0.27	9.11	0.25	Y
NGC1560	1.12	9.26	0.12	Y	0.79	9.22	0.13	Y	0.44	9.18	0.14	Y
NGC5585	0.72	9.38	0.18	Y	0.51	9.32	0.19	Y	0.29	9.25	0.21	Y
UGC7321	1.26	9.44	0.20	Y	0.89	9.38	0.21	Y	0.50	9.29	0.22	Y
UGC6818	0.64	9.49	0.11	N	0.45	9.42	0.11	Y	0.25	9.32	0.12	Y
UGC4499	0.67	9.36	0.15	Y	0.47	9.32	0.16	Y	0.27	9.27	0.18	Y
IC 2233	0.59	9.44	0.11	Y	0.42	9.38	0.11	Y	0.23	9.31	0.13	Y
F583-1	0.54	9.30	0.17	Y	0.39	9.28	0.18	Y	0.22	9.26	0.18	Y
NGC6503	1.12	9.79	0.11	N	0.79	9.69	0.10	N	0.44	9.55	0.11	Y
UGC6917	0.95	9.91	0.11	N	0.67	9.82	0.11	N	0.38	9.70	0.11	Y
NGC4010	0.99	10.11	0.11	N	0.70	10.02	0.11	N	0.39	9.88	0.11	Y
UGC6983	0.69	9.87	0.11	Y	0.49	9.80	0.11	Y	0.28	9.73	0.12	Y
NGC2403	0.54	9.94	0.11	Y	0.39	9.87	0.11	Y	0.22	9.79	0.12	Y
NGC4183	0.54	10.08	0.11	N	0.39	9.99	0.11	N	0.22	9.89	0.11	Y
F5741	1.59	10.04	0.09	N	1.12	9.96	0.10	Y	0.63	9.87	0.10	Y
F5681	1.16	9.95	0.12	Y	0.82	9.90	0.13	Y	0.46	9.84	0.14	Y
NGC3769	1.48	10.34	0.11	N	1.05	10.25	0.11	N	0.59	10.13	0.11	Y
NGC1003	1.03	10.41	0.20	N	0.73	10.32	0.19	N	0.41	10.19	0.19	Y
NGC5033	1.03	10.49	0.20	N	0.73	10.40	0.19	N	0.41	10.27	0.19	Y
NGC3198	0.64	10.45	0.11	Y	0.45	10.38	0.11	Y	0.25	10.30	0.12	Y
NGC2998	0.69	10.96	0.11	N	0.49	10.87	0.11	N	0.28	10.74	0.11	Y
NGC6674	1.12	11.06	0.13	N	0.79	10.97	0.13	N	0.44	10.84	0.13	Y

NOTE.—Not shown here are galaxies that are star dominated for all population models. They are not used to determine the BTF relation.

TABLE 4
BTF FIT TO GAS DOMINATED GALAXIES

Subsample	N	$x_{v M}$	$\sigma_{x_{v M}}$	$A_{v M}$	$\sigma_{A_{v M}}$	$\chi^2_{\nu,v M}$	$x_{M v}$	$\sigma_{x_{M v}}$	$A_{M v}$	$\sigma_{A_{M v}}$	$\chi^2_{\nu,M v}$	x_{bis}	A_{bis}	$\chi^2_{\nu,bis}$
Portinari-Kroupa	23	3.77	0.22	2.08	0.42	1.28	4.11	0.25	1.43	0.47	1.18	3.93	1.78	1.25
Portinari-Salpeter	14	3.59	0.40	2.44	0.73	1.42	4.37	0.50	1.02	0.91	1.46	3.94	1.79	1.46
Portinari-Kennicutt	26	3.74	0.21	2.14	0.41	2.01	4.33	0.26	0.99	0.50	1.85	4.01	1.62	1.99
Bell-Scaled Salpeter	23	3.77	0.20	2.09	0.39	1.41	4.09	0.23	1.47	0.45	1.31	3.93	1.80	1.37
Bell-Kroupa	26	3.72	0.20	2.17	0.40	2.30	4.36	0.25	0.94	0.49	2.10	4.01	1.61	2.27
Bell-Bottema	36	3.55	0.29	2.45	0.29	2.02	3.96	0.16	1.63	0.32	2.06	3.74	2.06	2.04

TABLE 5
DERIVED VALUES FROM THE BTF RELATION

Galaxy	M_b	M_s^a	Υ
	($\log M_\odot$)		(M_\odot/L_\odot)
KK98251	7.92	-7.50	-0.28
NGC2683	10.42	10.40	1.82
UGC6667	9.39	9.12	0.35
UGC6923	9.31	8.95	0.28
UGC6818	9.11	-8.21	-0.06
NGC7793	9.58	9.35	0.42
NGC3972	10.16	10.10	1.29
NGC4085	10.20	10.14	1.18
NGC6503	9.91	9.79	1.63
NGC3877	10.58	10.55	1.27
NGC4138	10.34	10.30	1.70
NGC247	9.77	9.57	0.63
UGC6973	10.62	10.59	4.38
NGC3917	10.21	10.13	0.84
UGC6917	9.85	9.62	0.76
NGC4217	10.66	10.62	1.52
NGC4051	10.47	10.42	0.70
NGC3953	11.04	11.03	2.55
NGC4010	10.02	9.82	0.73
NGC4013	10.65	10.60	1.92
NGC4100	10.47	10.41	0.99
NGC3949	10.53	10.46	1.20
NGC4183	9.85	9.33	0.17
NGC2903	10.69	10.63	1.44
NGC3521	10.77	10.71	1.97
NGC3769	9.95	9.14	0.14
NGC3893	10.64	10.55	1.14
NGC1003	9.86	-9.20	-0.10
NGC3726	10.56	10.43	0.72
NGC5033	10.81	10.74	2.69
NGC5907	10.98	10.93	3.52
NGC7331	11.15	11.12	2.39
NGC4088	10.58	10.42	0.65
NGC4157	10.72	10.62	1.43
NGC3992	11.18	11.14	3.06
NGC2998	10.96	10.78	0.67
NGC801	10.99	10.82	0.83
NGC5533	11.17	11.06	1.91
NGC2841	11.47	11.41	1.36
NGC6674	11.18	11.05	1.67
UGC2885	11.54	11.47	1.30

^aSometimes the baryonic mass from the BTF is less than the gas mass, leading to a negative stellar mass. This should happen occasionally because of scatter in the relation. In no case is the stellar mass significantly less than zero.